Influence of load dynamic response on the stability of microgrids during islanding transition

Influence of Load Dynamic Response on the Stability of Microgrids During Islanding Transition

Juan Diego Rios Penaloza, James Amankwah Adu, Alberto Borghetti, Fabio Napolitano,
Fabio Tossani, Carlo Alberto Nucci
Department of Electrical, Electronic and Information Engineering (DEI)
University of Bologna
Bologna, Italy
{juan.riospenaloza3,jamesamankwah.adu,alberto.borghetti,fabio.napolitano,fabio.tossani,carloalberto.nucci}@unibo.it

***Abstract*—Microgrids (MGs) are characterized by faster dynamics than conventional grid-connected distributions systems. This is in part due to the lack of inertia of inverter-interfaced distributed energy resources such as photovoltaic and energy storage systems. In this context, load dynamics considerably affects the transient stability performance of MGs, especially if disconnected from the main grid. The aim of the paper is to analyze the influence of the load composition in the transient stability assessment of a medium voltage MG during islanding transition. The MG we analyze consists of a photovoltaic power plant, two battery energy storage systems, a synchronous generator and different classes and types of load, which we consider representative for the problem of interest. The system is implemented in the EMTP-RV simulation environment. The importance of appropriate load modelling for the adequate analysis of the transient response of an islanding microgrid is also addressed and discussed.**

***Index Terms*—Distributed energy resources, Droop control, Islanding, Load composition, Load model, Microgrid.**

I. Introduction

The increasing deployment of inverter-interfaced distributed energy resources (DER) such as wind, photovoltaic (PV) and battery energy storage systems (BESS) reduces the inertia of the power system, resulting in larger frequency and voltage deviations due to power imbalances that could lead to the system instability. These phenomena are prone to occur especially during islanding transitions of microgrids.

In dynamic power system analysis performed by transmission and distribution system operators, loads are often represented using static models [1], [2]. However, in microgrids (MGs) with low inertia DERs the influence of the dynamic response of loads might be of great significance. Therefore, it is worth to analyze on the one hand the impact of load modelling techniques in the stability assessment, and on the other hand the influence of the load composition, particularly during islanding maneuvers.

In [3], [4] the results of unplanned islanding transitions in a real low voltage (LV) MG are presented. The experimental MG can adopt a single or multi master operation mode. In the single-master operation mode, one source is chosen to be controlled as voltage reference, while the remaining sources are operated in PQ mode (grid-connected). In the multi-master operation mode, two or more sources are chosen to be controlled as voltage references with a droop control strategy [5]. If the master function is disabled for all sources, i.e. they are continuously controlled in PQ mode, the system blackout is almost unavoidable after the islanding transition. This is due to the lack of inertia especially if all components, sources and loads, are connected to the system through power converters. In [6] the islanding transition of a medium voltage (MV) MG with two BESSs and different percentages of rotating and stationary load is analyzed. The results shown in [6] indicate that when the droop control of the inverters is implemented, the stability after the islanding transition can be maintained provided a large ratio of rotating loads is present. However, MGs may supply many different types of loads [7], thus the distinction of the loads into rotating or stationary without considering their specific dependence on the frequency and voltage supply may not be sufficiently comprehensive. In [8] a study of the effect of different types of loads on the dynamic response of a LV MG is presented. The study contemplates i) a three-phase fault and the recovery after clearance when the MG is in grid-connected mode, ii) a load step change in islanded mode, and iii) a load step change in grid-connected mode. The results show the large influence of the load characteristics on the MG stability in the first two cases. This paper extends the analysis to the islanding transition.

As MGs are relatively small systems, and thus voltage changes at DERs terminals largely influences neighboring loads, an accurate representation of the sensitivity of the loads with respect to the nodal voltage is required to evaluate the stability of the system [8], [9]. This specific characteristic of MGs is also exploited in various dynamic voltage control schemes, as those presented in, e.g., [10], [11]. In [10] a control strategy is proposed for islanded MGs in which the voltage setpoints of the DERs depend on the frequency deviation. If the frequency drops, the voltage setpoint decreases, in order to reduce the power consumption. Clearly the performance of the proposed strategy is affected by the load mix. Indeed, as the voltage dependency of loads decreases, the effect of this droop

Submitted to the 21st Power Systems Computation Conference (PSCC 2020).
The research activity is carried out in the framework of the PODCAST project (platform for the optimization of the distribution using data from smart meters and distributed storage systems), partially funded by MiSE (Italian Ministry for Economic Development).

voltage control becomes less efficient. In [11] the same principle is applied to a diesel generation unit in an isolated high voltage system, and some measurement results in real operating conditions are presented. As the voltage of the MG fluctuates during unplanned islanding transition, the load consumptions will also vary, even without any intentional voltage control, thus influencing the MG stability and the success of the islanding maneuver.

This paper asses the influence of load modelling and composition in the stability analysis of a MV MG during unplanned islanding transitions. Typical load models used by system operators in dynamic power system analysis are compared. Moreover, the influence of the load composition is appraised by means of a sensitivity analysis that shows the impact of the load parameters on the MG stability during the islanding phase, expressed in terms of the minimum of frequency and voltage values reached in the MG. The analysis is first carried out for a simple system and then extended to a realistic MV network in order to evaluate the general validity of the results. Different types of loads are connected to the MV MG during the islanding transition. Loads are categorized in four classes, namely residential, commercial, industrial, and agricultural. Each load class is composed by a combination of different elementary types of loads that we consider representative for the problem of interest. All the results are obtained by simulations performed in the EMTP-RV environment.

The paper is structured as follows. Section II provides an outline of the load models most used in dynamic transient analysis that will be adopted in this paper. In section III the control strategies applied to the DER units are summarized. Section IV and V presents the simulation cases for the different load modelling techniques and different load compositions, respectively. Section VI concludes the paper.

II. LOAD MODELLING AND LOAD COMPOSITION

This section aims at a) summarizing the load models adopted in this paper, selected among those typically adopted in steady state analysis and dynamic calculations according to the global survey presented in [1] and [2] and b) at describing the system considered as test case, along with the relevant load composition.

A. Static load models

Two of the most frequently used static load models are the exponential model, in which absorbed powers are expressed by (1) and (2), and the ZIP model in which absorbed powers are expressed by (3) and (4),

$$P = P_n \left(\frac{U}{U_n} \right)^{k_{pu}} \left(1 + k_{pf} \Delta f \right) \tag{1}$$

$$Q = Q_n \left(\frac{U}{U_n} \right)^{k_{qu}} \left(1 + k_{qf} \Delta f \right) \tag{2}$$

$$P = P_n \left[p_1 \left(\frac{U}{U_n} \right)^2 + p_2 \left(\frac{U}{U_n} \right) + p_3 \right] \tag{3}$$

$$Q = Q_n \left[q_1 \left(\frac{U}{U_n} \right)^2 + q_2 \left(\frac{U}{U_n} \right) + q_3 \right] \tag{4}$$

where: P and Q are the active and reactive powers at voltage U and frequency f; P_n and Q_n are the active and reactive powers at the rated voltage U_n and frequency f_n; Δf is the relative frequency deviation; k_{pu}, k_{qu}, k_{pf} and k_{qf} are the parameters of the exponential model for the load, and; p_1, p_2, p_3 and q_1, q_2 and q_3 represent the weights of the constant impedance, constant current and constant power components that constitute the ZIP model for the active and reactive power, respectively. Both sums of p_1, p_2, and p_3 and q_1, q_2 and q_3 are equal to one.

The other widely used static load models are the constant impedance, constant current and constant power [12].

B. Dynamic load models

Induction motors (IMs) constitute the most common type of dynamic loads connected to residential, commercial and industrial microgrids [13]. Two models will be used in this paper, namely the model available in the EMTP-RV library [14] (hereafter called EMTP-model), and the model represented by the steady-state equivalent circuit of the IM, shown in Fig. 1 (hereafter called *slip*-model) [15]. The EMTP-model represents the IM in the *dq*0-frame, making it very accurate as it represents the stator and rotor electrical transients, other than the mechanical one. The *slip*-model does not require such a transformation as it includes only the representation of mechanical transients, making it simpler.

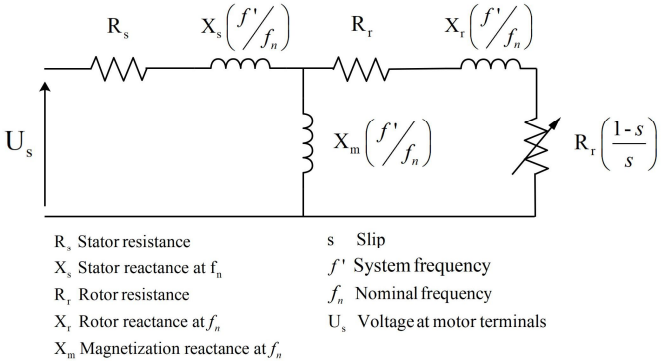

Fig. 1. Steady state equivalent circuit of the IM (*slip*-model).

C. Studied system

The studied system, as shown in Fig. 2, is a modified version of the Cigré benchmark for the integration of DERs in MV distribution networks [16], in which a synchronous generator (SG), a PV power station and two BESSs are included.

D. Load composition

As mentioned in the Introduction, loads are categorized in four classes, namely residential, commercial, industrial, and agricultural. Each load class is supposed to be composed by

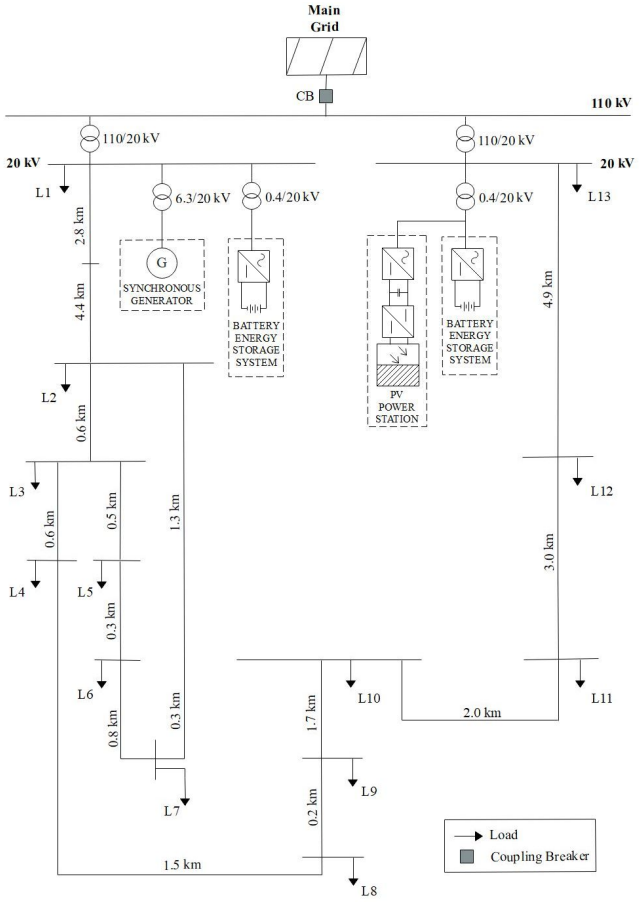

Fig. 2. Studied system: Modified version of the Cigré benchmark [16] for the integration of DERs in MV distribution networks.

different load components, as summarized in Table I. The load compositions of residential, commercial and industrial classes are based on the data reported in [17]–[20]. The agricultural load composition is assumed to be largely dominated by pumps; hence other load components are neglected. The power factor values are taken from [21]. The load parameters for each component for the different load models are reported in the Appendix. In particular, Table VIII of the Appendix shows the total load absorbed and the load class composition at each bus of the MG at the beginning of the considered islanding transition.

TABLE I. LOAD COMPOSITION FOR EACH OF THE CONSIDERED LOAD CLASSES

Load class	Load component	Power factor	%
Residential	Fan	0.87	5.0
	Refrigeration	0.84	10.0
	Air conditioner	0.75	50.0
	Washing machine	0.65	3.0
	Dryer	0.99	3.0
	Lighting	0.90	20.0
	Resistive loads	1.00	5.0
	TV	0.77	4.0
Commercial	Fan	0.87	11.9
	Refrigeration	0.84	13.4
	Air conditioner	0.75	14.9
	Pumps and other motors	0.87	5.5
	Office equipment	1.00	13.1
	Lighting	0.90	34.5
	Resistive loads	1.00	6.7
Industrial	Small motor	0.83	20.0
	Large motor	0.89	56.0
	Lighting	0.90	19.0
	Resistive loads	1.00	5.0
Agricultural	Agricultural pump	0.85	100.0

III. DISTRIBUTED ENERGY RESOURCES

This section describes the characteristics of the different DERs and storage units assumed to be installed in the MG.

A. Synchronous generator

The parameters of the SG are reported in Table II.

TABLE II. PARAMETERS OF THE SYNCHRONOUS GENERATOR

Rated Power	1 MVA
Rated Voltage	6.3 kV
Active power reference	1 pu
Active power droop	2.4 %
Inertia constant	1 s

B. PV power plant

The PV power plant is connected to the network through a DC-DC converter in cascade with an inverter. In the former, the perturb and observe technique of the maximum point power tracking (MPPT) strategy is implemented, while the latter is controlled to maintain the voltage at the DC-link constant. The PV unit is represented by the single-diode model as developed in [22]. The parameters of the PV unit are reported in Table III.

TABLE III. PARAMETERS OF THE PV POWER PLANT

Cell		Array	
Open-circuit (OC) voltage	32.9 V	**Num. cells per module**	54
Short-circuit (SC) current	8.21 A	**Num. modules in series**	44
Temp. coefficient OC	-0.123 V/°C	**Num. modules in parallel**	171
Temp. coefficient SC	0.00318 A/°C	**Series resistance**	0.083 Ω
Diode ideality constant	1.025	**Parallel resistance**	43.404 Ω

Both power converters are represented by the average model [23], [24], which is considered suitable for determining the frequency transients of the network [25].

C. Battery energy storage system

The dynamic response of the battery is modelled by three RC branches in series with the battery resistance, which parameter values are reported in [26]. Such values depend on the state of charge, which is assumed to remain constant during the transients considered in this paper, as in [27].

The power converters of both BESSs are controlled in the PQ-mode with a droop control strategy, as shown in Fig. 3. The droop control modifies the power reference in order to respond accordingly to generation/load variations as follows

$$P^* = P_{ref} + \frac{1}{k_P}\left(f_{ref} - f\right) \tag{5}$$

$$Q^* = Q_{ref} + \frac{1}{k_Q}\left(v_{ref} - v\right) \tag{6}$$

where f_{ref}, v_{ref}, P_{ref}, and Q_{ref} are the reference values for the frequency, voltage, active and reactive powers, respectively, k_P and k_Q are the droop constants for active and reactive power control, respectively and, P^* and Q^* are the reference values modified by the droop control. The power converter, as for the PV power plant, is represented by the average model. The parameters of the BESS are reported in Table IV.

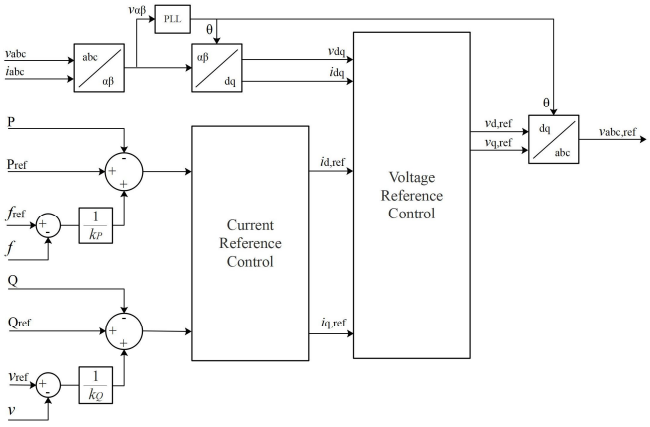

Fig. 3. Control scheme of the power converters of the BESSs.

TABLE IV. PARAMETERS OF THE BESS

Rated power	1 MVA
Rated voltage	0.4 kV
Active power droop (k_P)	2.4 %
Reactive power droop (k_Q)	10.0 %
Active power reference (P_{ref})	0 pu
Reactive power reference (Q_{ref})	0 pu
Frequency reference (f_{ref})	50 Hz
Voltage reference (v_{ref})	1 pu

IV. INFLUENCE OF LOAD MODELLING

In this section the influence of load modelling during the islanding transition of the MG is analyzed. The 6 cases reported in Table V are simulated and the relevant frequency and voltage transients are compared. The load representation in the *Exp+EMTP* case is the most detailed therefore this case is taken as benchmark. The transients are initiated by a three-phase fault in the main grid at t=0 s followed by the opening of the coupling breaker (CB) after 50 ms. The base case load composition of Table VIII is considered.

TABLE V. STUDY CASES FOR ASSESSING THE INFLUENCE OF LOAD MODELLING

Case models	Load representation
Exp+EMTP	Stationary loads are represented by the exponential model. Rotating loads are represented by the EMTP-model of the IM.
Exp+slip	Stationary loads are represented by the exponential model. Rotating loads are represented by the slip-model of the IM.
ZIP+slip	Stationary loads are represented by the ZIP model. Rotating loads are represented by the slip-model of the IM.
Exp	Stationary and rotating loads are represented by the exponential model.
P	Stationary and rotating loads are represented as constant power loads.
Z	Stationary and rotating loads are represented as constant impedance loads.

Dynamic loads are controlled to provide constant mechanical torque during the entire simulation.

With the *P*-model, the islanding transition leads to the system instability. For all the other models this does not occur: the frequency and voltage transients are shown in Fig. 4 and Fig. 5. After the islanding transition the frequency and the voltage steady state values differ from the nominal values because of the droop strategy adopted. The frequency and voltage deviation is proportional to the active and reactive power supplied by the DERs, as can be deduced from (5) and (6). Typically, secondary frequency and voltage control layers, not included in the model, are responsible of taking these values back to the rated settings. The same frequency and voltage late time values are obtained by using all the models except the *Z*-model that presents a slightly different frequency value, as shown by Fig. 4b). By using the *Exp+slip* and the *ZIP+slip* models, the representation of the frequency transient well matches the reference one. It is worth noting that there are not significant differences between the *Exp+slip* and the *ZIP+slip* models during the transient and in the late time response.

In order to analyze the frequency and voltage transients in a system in which all DER units are inertia-less, the SG is

disconnected from the MG. Then, the same fault is simulated at t=0 s, followed by the islanding transition after 50 ms.

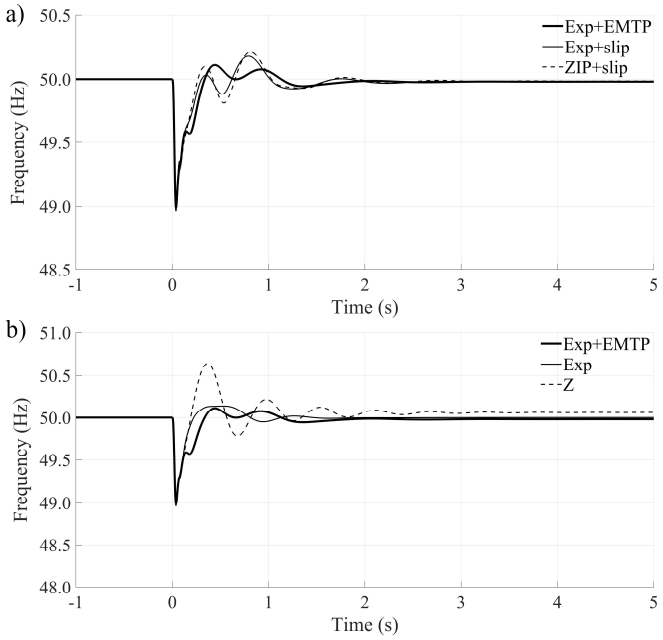

Fig. 4. Frequency transient during islanding transition. SG is connected to the MG.

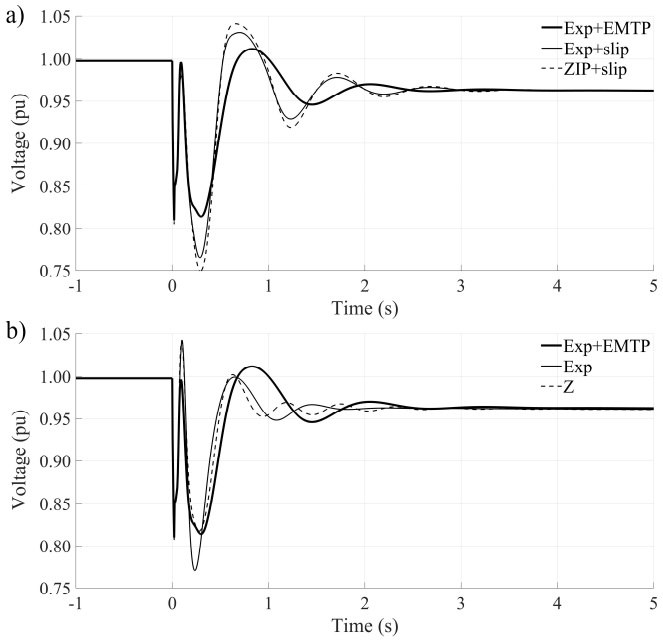

Fig. 5. Voltage transient during islanding transition. SG is connected to the MG.

As the aim is the assessment of the influence of the load dynamic response during the islanding transition of the MG, the change of control strategy of the BESS from PQ to Vf-mode (which normally should take place to guarantee a proper operation in standalone when all DER units are inverter-connected) is deliberately disregarded.

The simulation results show that when all loads are represented by some static model, namely by the *Exp*, *P* or *Z* models, the islanding transition leads to the system instability. For the cases in which the dynamic representation of the load is included, the frequency and voltage transients are shown in Fig. 6.

In this case, the *Exp+slip* and *ZIP+slip* models are accurate enough to represent the transient response during the islanding transition of the considered MG. The steady state values after the disturbance are equal for the three cases. Since the exponential model is simpler than the *ZIP*-model, the *Exp+slip* model might be preferred.

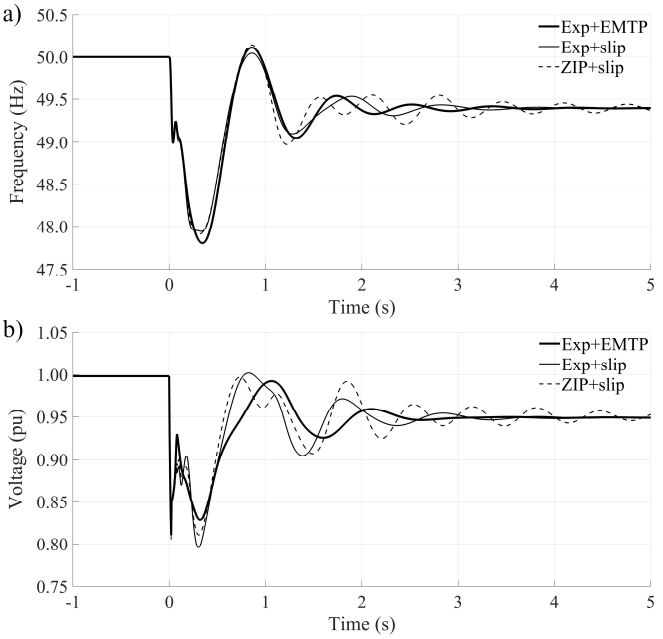

Fig. 6. a) Frequency and b) voltage transients during islanding transition. SG is disconnected from the MG.

V. INFLUENCE OF LOAD COMPOSITION

This section focuses on the analysis of the influence of the load composition. First, a sensitivity analysis is carried out in a small system, in which the influence of the main load parameters in the frequency and voltage transients is compared. Afterwards, the analysis is extended to the complete system of Fig. 2.

A. Sensitivity analysis

The analysis is carried out considering the system shown in Fig. 7. Loads are consisting of stationary and rotating loads, represented by the exponential and the EMTP models, respectively. The base values are $k_{pu} = k_{qu} = 1$, $k_{pf} = k_{qf} = 0$, $H = 1$ s and 50% of rotating load. Before islanding, the MG was importing both active and reactive power. The islanding transition begins with the opening of the CB. The fault in this case is not simulated.

First, we analyze the influence of the inertia constant of the rotating loads. Fig. 8 shows the minimum values of frequency and voltage during the islanding transition. Both increase as the

inertia constant increases. However, the voltage increase is limited. For values of H less than 0.5, the system is unstable.

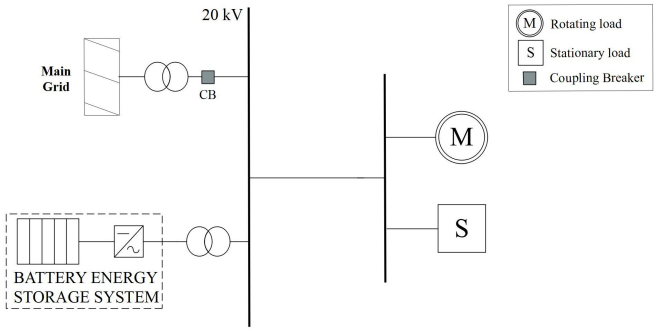

Fig. 7. Simple MV system containing a BESS and rotating and stationary loads.

Subsequently, we analyze the influence of the percentage of rotating load (η_{rot}), assuming H = 1.5 s. Fig. 9 shows the minimum values of frequency and voltages. Both increase with the increasing of the rotating load percentage. For load compositions with less than 35% of rotating load, the system is unstable.

Finally, we analyze the influence of k_{pu}, k_{qu}, k_{pf} and k_{qf}. Figs. from 10 to 13 show the minimum values of frequency and voltage during the islanding transition. The minimum frequency increases when k_{pu} or k_{pf} increase (Fig. 10a and Fig. 12a) and decrease when k_{qu} or k_{qf} increase (Fig. 11a and Fig. 13a). As shown by Fig. 10b, Fig. 11b and Fig. 13b, the increase of k_{pu}, k_{qu} or k_{qf} leads to an increase of the minimum voltage, while k_{pf} has a negligible influence on it.

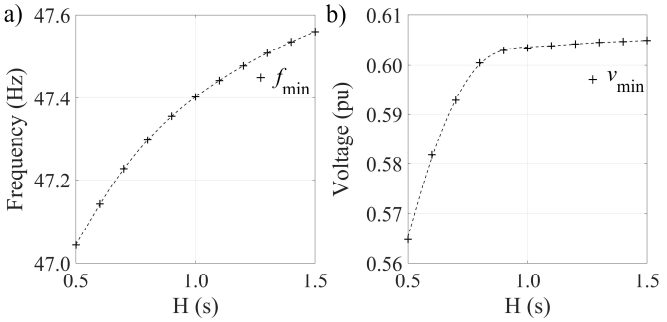

Fig. 8. Influence of inertia constant H on a) frequency and b) voltage transients during the islanding transition.

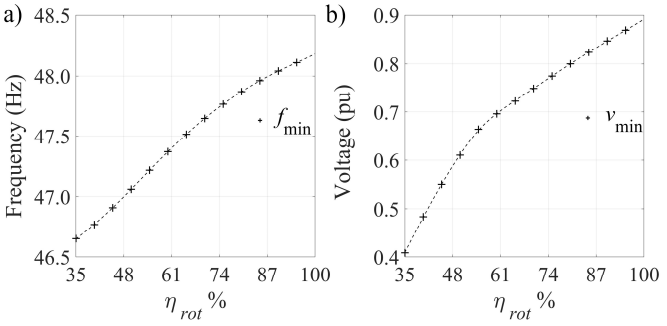

Fig. 9. Influence of the percentage of rotating load on a) frequency and b) voltage transients during the islanding transition.

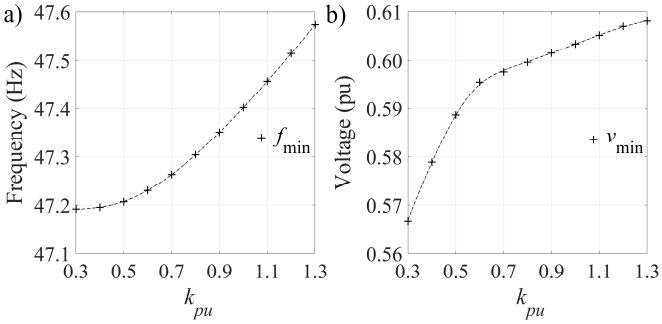

Fig. 10. Influence of parameter k_{pu} on a) frequency and b) voltage transients during the islanding transition.

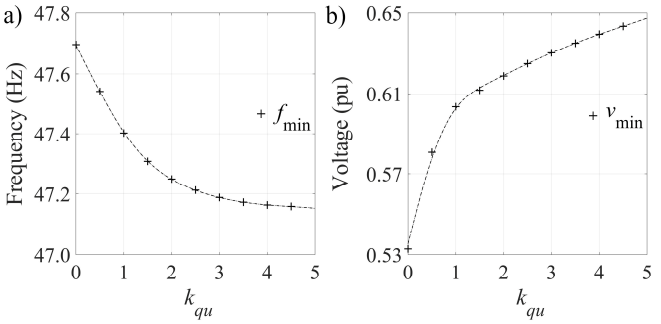

Fig. 11. Influence of parameter k_{qu} on a) frequency and b) voltage transients during the islanding transition.

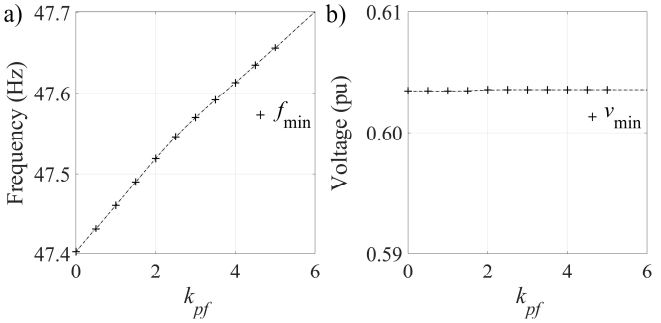

Fig. 12. Influence of parameter k_{pf} on a) frequency and b) voltage transients during the islanding transition.

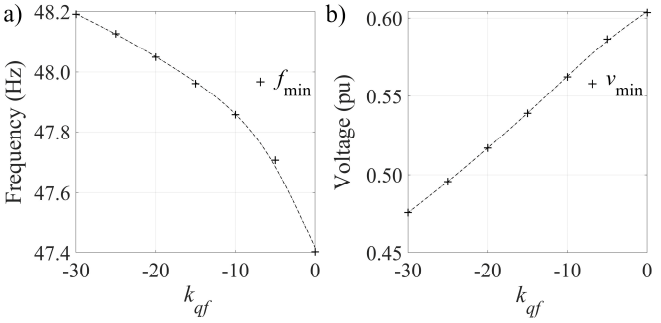

Fig. 13. Influence of parameter k_{qf} on a) frequency and b) voltage transients during the islanding transition.

B. Study cases

Now we extend the above analysis to the network of Fig. 2. The load composition is characterized by estimating representative values for H, k_{pu}, k_{qu} k_{pf} and k_{qf}. The equivalent inertia constant H_{eq} is estimated, according to [28], as

$$H_{eq} = \sum_i s_{i,rot} H_i \tag{7}$$

where $s_{i,rot}$ is the portion of load (apparent power) of type i with inertia H_i with respect to the total rotating load. It is worth noting that this equivalent is referred only to the rotating load. The inertia constant of the entire system instead, would be expressed as

$$H_{sys} = \sum_i s_i H_i = H_{eq} \eta_{rot} \tag{8}$$

where s_i is the portion of load of type i with inertia H_i with respect to the total load. The exponential parameters $k_{pu,eq}$, $k_{qu,eq}$, $k_{pf,eq}$ and $k_{qf,eq}$ are estimated from an equivalent characteristic such that

$$V^{k_{pu,eq}} = \sum_i p_{i,st} V^{k_{pu,i}} \tag{9}$$

$$V^{k_{qu,eq}} = \sum_i q_{i,st} V^{k_{qu,i}} \tag{10}$$

$$1 + k_{pf,eq}\,\Delta f = \sum_i p_{i,st}(1 + k_{pf,i}\,\Delta f) \tag{11}$$

$$1 + k_{qf,eq}\,\Delta f = \sum_i q_{i,st}(1 + k_{qf,i}\,\Delta f) \tag{12}$$

where $p_{i,st}$ ($q_{i,st}$) is the portion of active (reactive) power absorbed by the load of type i with exponential parameters $k_{pu,i}$ $k_{qu,i}$, $k_{pf,i}$ and $k_{qf,i}$ with respect to the total stationary active (reactive) power.

The equivalent parameters and percentage of rotating load of the residential, commercial, industrial, and agricultural classes of load are shown in Table VI.

The percentages of load classes in each bus were varied keeping constant the total load. The equivalent parameters and the obtained results for all cases are presented in Table VII.

From Cases A to D parameters that improve stability, i.e. H_{eq}, η_{rot}, k_{pu}, k_{pf}, increase, while those worsening it, i.e. k_{qu} and k_{qf}, decrease, so from A to D the frequency and the voltage responses improve in terms of minimum reached values, as shown by the results of Table VII.

Cases E to H have a 40% increase of residential, commercial, industrial, and agricultural loads, respect to the *Base* case of Table VIII. Although Case F has a larger H_{eq} than Case E, the minimum frequency is smaller. This can be attributed mainly to the lower value of rotating load, but also to the lower value of $k_{pu,eq}$ and the larger value of $k_{qu,eq}$. The best case in terms of minimum frequency and voltage is Case G, in which the industrial load is predominant. Such result might be attributed to the very large H_{eq} and the relatively high percentage of rotating load. Case H too, in which the agricultural load is predominant, results in a smaller frequency deviation.

In Fig. 14 and Fig. 15 the frequency and voltage minimum values with respect to H_{sys} are shown. It is evident how the minimum frequency increases with the increasing of the total system inertia, regardless of the other parameters. The same occurs for the minimum voltage, except for case E.

TABLE VI. EQUIVALENT PARAMETERS OF ALL LOAD CLASSES

Case	H_{eq}	η_{rot}	$k_{pu,eq}$	$k_{qu,eq}$	$k_{pf,eq}$	$k_{qf,eq}$
Residential	0.320	71.0	1.21	6.94	0.69	-21.62
Commercial	0.440	45.7	0.86	7.38	0.61	-26.60
Industrial	1.289	76.0	1.14	7.38	0.77	-26.60
Agricultural	0.800	100.0	-	-	-	-

TABLE VII. STUDY CASES. EQUIVALENT PARAMETERS AND MINIMUM FREQUENCY AND VOLTAGE VALUES

Case	H_{eq}	η_{rot}	$k_{pu,eq}$	$k_{qu,eq}$	$k_{pf,eq}$	$k_{qf,eq}$	f_{min}	v_{min}
A	0.689	59.2	0.91	7.33	0.64	-26.02	48.83	0.810
B	0.796	67.6	1.00	7.26	0.67	-25.19	48.97	0.819
C	0.844	75.1	1.08	7.21	0.70	-24.62	49.04	0.825
D	0.893	78.3	1.17	7.18	0.74	-24.23	49.08	0.830
E	0.622	74.6	1.17	7.05	0.70	-22.85	48.95	0.800
F	0.689	59.2	0.91	7.33	0.64	-26.02	48.83	0.810
G	1.037	75.0	1.10	7.28	0.73	-25.46	49.11	0.842
H	0.796	86.4	1.07	7.19	0.69	-24.43	48.05	0.826

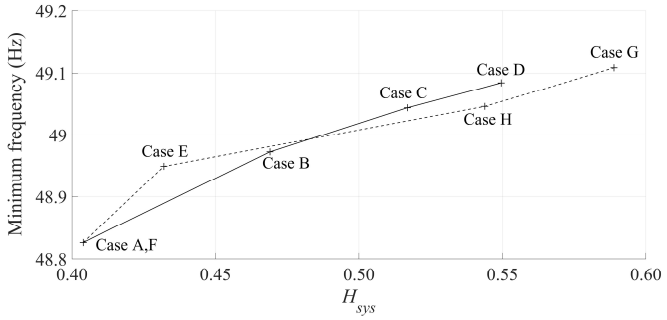

Fig. 14. Minimum frequency values reached during the islanding transition, as reported on Table VII.

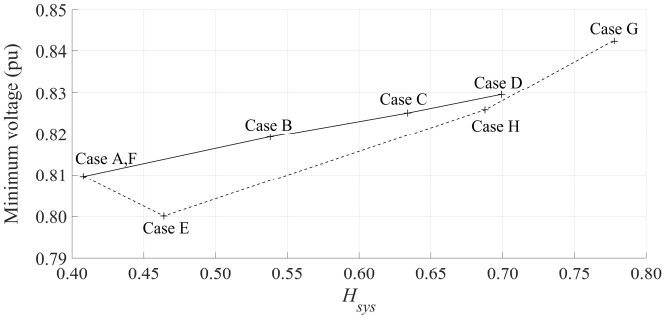

Fig. 15. Minimum voltage values reached during the islanding transition, as reported on Table VII.

VI. CONCLUSIONS

The paper has analyzed the influence of load modeling and composition on the transient stability of a MV MG during islanding transitions. The considered MG consists of a PV power plant, two BESSs, a SG and different types of loads which are categorized in four classes, namely residential, commercial, industrial and agricultural, in which each load class is composed by different stationary and rotating load components.

The influence of load modelling on the MG stability assessment during islanding transition has been addressed by taking as reference the results of the *EMTP*-model. If the SG is connected to the MG, which is the only DER with rotating inertia, all models except for the *P*-model predict the stability of the MG after islanding. There are no substantial differences between the *Exp*+*slip* and *ZIP*+*slip* models. While these two models are more accurate to represent the frequency transient, the *Exp* model performs better if one is interested in representing the voltage transient. However, if the SG is not connected to the MG, the *Exp* and *Z* models predict the system instability. In such a case, only the *Exp*+*slip* and *ZIP*+*slip* models, i.e. the models that include the rotating nature of the loads, are accurate enough to represent the stable transient response of the MG

Concerning the load composition, the increase of H, k_{pu} and the percentage of rotating load improves the power quality during the islanding maneuver in terms of minimum frequency and voltage variations. The increase of k_{qu} instead, worsen the voltage profile but improves the frequency nadir.

The analysis was extended to the modified version of a Cigré benchmark system. For such purpose, the percentages of load classes in each bus is varied keeping constant the total load. The load dynamic response of the system is represented by equivalent parameters H_{eq}, $k_{pu,eq}$ and $k_{qu,eq}$. The results agree with those obtained with the smaller system. In particular, the considered industrial and agricultural classes of load are more prone to ease the islanding transition with respect to the residential and commercial classes, due to their larger values of equivalent inertia and percentage of rotating load.

APPENDIX

The total load and load composition for each bus of the system of Fig. 2 are reported in Table VIII.

Table IX shows the IM load model parameters of the considered rotating load components. The parameters refer to the circuit of Fig. 1 and H represents the inertia constant. Table IX also shows the load parameters of all the considered load components, stationary and rotating, for the exponential and the ZIP models. Reference is made to equations (1)-(4). The load parameters are based on diverse data found in literature [12], [21], [29]–[33].

TABLE VIII. LOAD COMPOSITION AND TOTAL LOAD ABSORPTION AT EACH BUS OF THE MG

Load bus		**L1**	**L2**	**L3**	**L4**	**L5**	**L6**	**L7**	**L8**	**L9**	**L10**	**L11**	**L12**	**L13**
Total load (kVA)		450	167	90	270	180	90	108	243	180	126	270	315	450
Case	**Class (%)**													
Base	Residential	0	0	70	100	50	100	50	40	70	50	0	0	0
	Commercial	20	10	30	0	50	0	50	60	30	10	10	20	0
	Industrial	80	40	0	0	0	0	0	0	0	40	50	0	80
	Agricultural	0	50	0	0	0	0	0	0	0	0	40	80	20
Case A and F	Residential	0	0	30	60	10	60	10	0	30	30	0	0	0
	Commercial	60	50	70	40	90	40	90	100	70	50	50	60	40
	Industrial	40	20	0	0	0	0	0	0	0	20	30	0	60
	Agricultural	0	30	0	0	0	0	0	0	0	0	20	40	0
Case B	Residential	0	30	30	90	10	90	10	30	30	60	0	0	30
	Commercial	30	20	40	10	60	10	60	70	40	20	20	30	10
	Industrial	70	20	30	0	30	0	30	0	30	20	60	30	60
	Agricultural	0	30	0	0	0	0	0	0	0	0	20	40	0
Case C	Residential	0	50	30	80	0	80	0	30	30	60	20	30	30
	Commercial	20	0	0	0	30	0	30	50	20	0	0	0	0
	Industrial	80	20	40	0	40	0	40	0	30	40	60	30	70
	Agricultural	0	30	30	20	30	20	30	20	20	0	20	40	0
Case D	Residential	0	70	0	70	30	60	30	50	30	60	20	30	30
	Commercial	0	0	0	0	0	0	0	0	0	0	0	0	0
	Industrial	100	0	70	30	40	20	40	30	30	40	60	30	70
	Agricultural	0	30	30	0	30	20	30	20	40	0	20	40	0
Case E	Residential	40	40	100	100	90	100	90	80	100	90	40	40	40
	Commercial	0	0	0	0	10	0	10	20	0	0	0	0	0
	Industrial	60	25	0	0	0	0	0	0	0	10	35	0	60
	Agricultural	0	35	0	0	0	0	0	0	0	0	25	60	0
Case G	Residential	0	0	50	60	30	60	30	20	50	20	0	0	0
	Commercial	0	0	10	0	30	0	30	40	10	0	0	0	0
	Industrial	100	80	40	40	40	40	40	40	40	80	90	40	100
	Agricultural	0	20	0	0	0	0	0	0	0	0	10	60	0
Case H	Residential	0	0	50	60	30	60	30	20	50	35	0	0	0
	Commercial	0	0	10	0	30	0	30	40	10	0	0	0	0
	Industrial	60	10	0	0	0	0	0	0	0	25	20	0	40
	Agricultural	40	90	40	40	40	40	40	40	40	40	80	100	60

TABLE IX. LOAD PARAMETERS [12], [21], [29]–[33]

Load component	R_s	X_s	X_m	R_r	X_r	H (s)	k_{pu}	k_{qu}	k_{pf}	k_{qf}	p_1	p_2	p_3	q_1	q_2	q_3
Lighting	-	-	-	-	-	-	0.96	7.38	1.00	-26.60	0.58	0.53	-0.11	8.04	-11.42	4.38
Resistive loads	-	-	-	-	-	-	2.00	0.00	0.00	0.00	0.92	0.10	-0.02	0.00	0.00	0.00
TV	-	-	-	-	-	-	2.00	5.20	0.00	-4.60	0.33	-0.57	1.24	19.00	-33.22	15.22
Office equipment	-	-	-	-	-	-	0.36	0.00	0.00	0.00	0.34	-0.32	0.98	0.00	0.00	0.00
Washing machine	0.110	0.120	2.0	0.110	0.130	0.69	0.08	1.60	3.00	1.80	0.05	0.31	0.63	-0.56	2.20	-0.65
Dryer	0.120	0.150	1.9	0.130	0.140	0.11	2.04	3.27	0.00	-2.63	1.96	-2.23	1.33	2.51	-2.34	0.83
Refrigerator	0.056	0.087	2.4	0.053	0.082	0.28	0.77	2.50	0.53	-1.46	1.19	-0.26	0.07	0.59	0.65	-0.24
Air conditioner	0.100	0.100	1.8	0.090	0.060	0.28	0.20	2.30	0.90	-2.67	1.60	-2.69	2.09	12.53	-21.11	9.58
Fan	0.079	0.120	3.2	0.052	0.120	0.70	0.08	1.60	2.90	1.80	0.26	0.90	-0.16	0.50	0.62	-0.12
Pumps and motors	0.079	0.120	3.2	0.052	0.120	0.70	0.08	1.60	2.90	1.80	0.46	0.73	-0.19	2.17	-3.03	1.87
Small indust. motors	0.031	0.100	3.2	0.018	0.180	0.70	0.07	0.50	2.50	1.20	1.35	-0.98	0.63	2.31	-3.72	2.40
Large indust. motors	0.013	0.067	3.8	0.009	0.170	1.50	0.07	0.50	2.50	1.20	0.48	0.78	-0.26	2.01	-2.70	1.70
Agricultural pumps	0.025	0.088	3.2	0.016	0.170	0.80	1.40	1.40	5.00	4.00	0.46	0.73	-0.19	2.17	-3.03	1.87

REFERENCES

[1] Cigré Working Group C4.605, "Modelling and Aggregation of Loads in Flexible Power Networks," CIGRE, Paris, France, Tech. Brochure 566, 2014.

[2] J. V. Milanović, K. Yamashita, S. Martínez Villanueva, S. Ž. Djokić, and L. M. Korunović, "International industry practice on power system load modeling," *IEEE Trans. Power Syst.*, vol. 28, no. 3, pp. 3038–3046, 2013.

[3] A. Cagnano, E. De Tuglie, and L. Cicognani, "Prince — Electrical Energy Systems Lab: A pilot project for smart microgrids," *Electr. Power Syst. Res.*, vol. 148, pp. 10–17, 2017.

[4] A. Cagnano, E. De Tuglie, M. Dicorato, G. Forte, and M. Trovato, "PrInCE Lab experimental microgrid Planning and operation issues," in *2015 IEEE 15th International Conference on Environment and Electrical Engineering, EEEIC 2015 - Conference Proceedings*, 2015.

[5] J. A. P. Lopes, C. L. Moreira, and A. G. Madureira, "Defining Control Strategies for MicroGrids Islanded Operation," *IEEE Trans. Power Syst.*, vol. 21, no. 2, pp. 916–924, 2006.

[6] J. D. Rios Penaloza, J. A. Adu, A. Borghetti, F. Napolitano, F. Tossani, and C. A. Nucci, "A Power Control Scheme for the Islanding Transition of a Microgrid with Battery Energy Storage Systems," in *19th EEEIC Environment and Electrical Engineering International Conference*, 2019.

[7] A. Hirsch, Y. Parag, and J. Guerrero, "Microgrids: A review of technologies, key drivers, and outstanding issues," *Renew. Sustain. Energy Rev.*, no. 90, pp. 402–411, 2018.

[8] IEEE PES Task Force on Microgrid Stability Analysis and Modeling, "Microgrid Stability Definitions, Analysis, and Modeling," IEEE PES, Technical Report PES-TR66, 2018.

[9] IEEE PES Task Force on Microgrid Stability Analysis and Modeling, "Microgrid Stability Definitions, Analysis, and Examples," *IEEE Trans. Power Syst. (Early Access)*, 2019.

[10] M. Farrokhabadi, C. A. Cañizares, and K. Bhattacharya, "Frequency control in isolated/islanded microgrids through voltage regulation," *IEEE Trans. Smart Grid*, vol. 8, no. 3, pp. 1185–1194, 2017.

[11] G. Delille, L. Capely, D. Souque, and C. Ferrouillat, "Experimental validation of a novel approach to stabilize power system frequency by taking advantage of Load Voltage Sensitivity," in *2015 IEEE Eindhoven PowerTech, PowerTech 2015*, 2015.

[12] P. Kundur, *Power System Stability and Control*. McGraw-Hill Education, 1994.

[13] N. Hatziargyriou, *Microgrids: Architectures and Control*. John Wiley and Sons Ltd, 2014.

[14] H. W. Dommel, *Electromagnetic Transients Program Theory Book*. Bonneville Power Administration, 1986.

[15] D. S. Brereton, D. G. Lewis, and C. C. Young, "Representation of Induction-Motor Loads During Power-System Stability Studies," *Trans. Am. Inst. Electr. Eng. Part III Power Appar. Syst.*, pp. 451–460, 1957.

[16] CIGRE Working Group C4.605, "Benchmark Systems for Network Integration of Renewable and Distributed Energy Resources," CIGRE, Paris, France, Tech. Rep. C6.04.02, 2014.

[17] Itron Inc, "California commercial end-use survey," Consultant Report, CEC-400-2006-005, 2006.

[18] California Energy Commission, "Attachment 13. References for Energy End-Use, Electricity Demand and GHG Emissions Reference and Calculations. March 1042014. PON-13-301. EPIC Grant program.," Sacramento, 2014.

[19] K. Morison, H. Hamadani, and L. Wang, "Load modeling for voltage stability studies," in *2006 IEEE PES Power Systems Conference and Exposition, PSCE 2006 - Proceedings*, 2006.

[20] "Comprehensive Load Modeling for System Planning Studies," EPRI, Palo Alto, CA, 2009.

[21] C. W. Taylor, *Power System Voltage Stability*. Palo Alto: EPRI Editors, 1994.

[22] M. G. Villalva, J. R. Gazoli, and E. R. Filho, "Comprehensive approach to modeling and simulation of photovoltaic arrays," *IEEE Trans. Power Electron.*, vol. 24, no. 5, pp. 1198–1208, 2009.

[23] J. Peralta, H. Saad, S. Dennetière, J. Mahseredjian, and S. Nguefeu, "Detailed and averaged models for a 401-level MMC-HVDC system," *IEEE Trans. Power Deliv.*, vol. 27, no. 3, pp. 1501–1508, 2012.

[24] Y. Che, W. Li, X. Li, J. Zhou, S. Li, and X. Xi, "An improved coordinated control strategy for PV system integration with VSC-MVDC technology," *Energies, MDPI*, vol. 10, no. 1670, pp. 1–14, 2017.

[25] H. Jin, "Behavior-mode simulation of power electronic circuits," *IEEE Trans. Power Electron.*, vol. 12, no. 3, pp. 443–452, 1997.

[26] F. Sossan, E. Namor, R. Cherkaoui, and M. Paolone, "Achieving the Dispatchability of Distribution Feeders Through Prosumers Data Driven Forecasting and Model Predictive Control of Electrochemical Storage," *IEEE Trans. Sustain. Energy*, vol. 7, no. 4, pp. 1762–1777, 2016.

[27] U. Datta, A. Kalam, and J. Shi, "Battery Energy Storage System to Stabilize Transient Voltage and Frequency and Enhance Power Export Capability," *IEEE Trans. Power Syst.*, vol. 34, no. 3, pp. 1845–1857, 2018.

[28] P. Tielens and D. Van Hertem, "The relevance of inertia in power systems," *Renew. Sustain. Energy Rev.*, no. 55, pp. 999–1009, 2016.

[29] J. R. Ribeiro and F. J. Lange, "A new aggregation method for determining composite load characteristics," *IEEE Trans. Power Appar. Syst.*, vol. PAS-101, no. 8, pp. 2869–2875, 1982.

[30] L. M. Hajagos, "Laboratory measurements and models of modern loads and their effect on voltage stability studies," *IEEE Trans. Power Syst.*, vol. 13, no. 2, pp. 584–592, 1998.

[31] L. Korunović and D. Stojanović, "Load Model Parameters on Low and Medium Voltage in Distribution Networks," *Elektroprivreda*, vol. 55, no. 2, pp. 46–56, 2002.

[32] A. Bokhari, A. Alkan, R. Dogan, M. Diaz-Aguilo, F. De Leon, D. Czarkowski, Z. Zabar, L. Birenbaum, A. Noel, and R. E. Uosef, "Experimental determination of the ZIP coefficients for modern residential, commercial, and industrial loads," *IEEE Trans. Power Deliv.*, vol. 29, no. 3, pp. 1372–1381, 2014.

[33] "Advanced Load Modeling," EPRI, Palo Alto, CA, and Public Service Company of New Mexico, Albuquerque, 2002.